

## Superhydrophilicity of $\alpha$ -alumina surfaces results from tight binding of interfacial waters to specific aluminols



Ruiyu Wang <sup>a,b,\*</sup>, Yunqian Zou <sup>a</sup>, Richard C. Remsing <sup>c</sup>, Naomi O. Ross <sup>a</sup>, Michael L. Klein <sup>a,b,d</sup>, Vincenzo Carnevale <sup>d,e,\*</sup>, Eric Borguet <sup>a,b,\*</sup>

<sup>a</sup> Department of Chemistry, Temple University, Philadelphia, PA 19122, United States

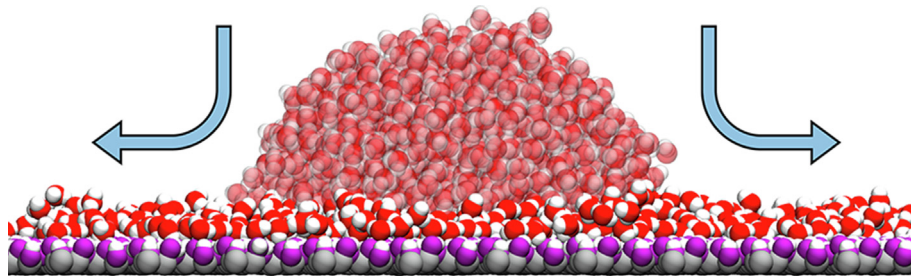
<sup>b</sup> Center for Complex Materials from First Principles (CCM), Temple University, 1925 North 12th Street, Philadelphia, PA 19122, United States

<sup>c</sup> Department of Chemistry and Chemical Biology, Rutgers University, Piscataway, NJ 08854, United States

<sup>d</sup> Institute for Computational Molecular Science, Temple University, Philadelphia, PA 19122, United States

<sup>e</sup> Department of Biology, Temple University, Philadelphia, PA 19122, United States

### GRAPHICAL ABSTRACT



### ARTICLE INFO

#### Article history:

Received 19 April 2022

Revised 25 July 2022

Accepted 26 July 2022

Available online 30 July 2022

#### Keywords:

Water

Alumina

Molecular Dynamics Simulation

Contact Angle

Wetting

### ABSTRACT

**Hypothesis:** Understanding the microscopic driving force of water wetting is challenging and important for design of materials. The relations between structure, dynamics and hydrogen bonds of interfacial water can be investigated using molecular dynamics simulations.

**Experiments and simulations:** Contact angles at the alumina (0001) and (11 $\bar{2}$ 0) surfaces are studied using both classical molecular dynamics simulations and experiments. To test the superhydrophilicity, the free energy cost of removing waters near the interfaces are calculated using the density fluctuations method. The strength of hydrogen bonds is determined by their lifetime and geometry.

**Findings:** Both surfaces are superhydrophilic and the (0001) surface is more hydrophilic. Interactions between surfaces and interfacial waters promote a templating effect whereby the latter are aligned in a pattern that follows the underlying lattice of the surfaces. Translational and rotational dynamics of interfacial water molecules are slower than in bulk water. Hydrogen bonds between water and both surfaces are asymmetric, water-to-aluminol ones are stronger than aluminol-to-water ones. Molecular dynamics simulations eliminate the impacts of surface contamination when measuring contact angles and the results reveal the microscopic origin of the macroscopic superhydrophilicity of alumina surfaces: strong water-to-aluminol hydrogen bonds.

© 2022 Published by Elsevier Inc.

\* Corresponding authors at: Department of Chemistry, Temple University, Philadelphia, PA 19122, United States (R. Wang and E. Borguet). Institute for Computational Molecular Science, Temple University, Philadelphia, PA 19122, United States (V. Carnevale).

E-mail addresses: [ruiyuwang@temple.edu](mailto:ruiyuwang@temple.edu) (R. Wang), [vincenzo.carnevale@temple.edu](mailto:vincenzo.carnevale@temple.edu) (V. Carnevale), [eborguet@temple.edu](mailto:eborguet@temple.edu) (E. Borguet).

## 1. Introduction

Water is one of the most important substances [1–4] and water/oxide interfaces are ubiquitous on earth, playing important roles in numerous chemical, physical, geological, and biological processes [5–8], such as mineral degradation [9,10], heterogeneous catalysis [11], phase transitions [12], solute adsorption [13,14] and wetting [15,16]. Investigating the behavior of interfacial waters is essential to help the design and development of better materials to overcome the energy crisis or increase their biological compatibility [17–21].

Among oxide surfaces,  $\alpha$ -alumina (corundum), the most stable form of  $\text{Al}_2\text{O}_3$ , has wide applications in ceramics industries [22], as catalyst supports [23] and as desiccants [24]. Interest in water/ $\alpha$ -alumina interfaces has grown in recent years. Using X-ray reflectivity measurements, water local density at alumina interfaces was measured and water ordering was found to be correlated with the crystalline orientation of the surfaces [25]. Both strongly and weakly hydrogen bonded (H-bonded) interfacial waters were observed in vibrational sum frequency spectra (SFG) [26–29]. In addition to these experimental studies, both classical and ab initio molecular dynamics (MD) simulations were carried out to study water adsorption [30], atomic force spectroscopic data [31], ion adsorption [24], the vibrational spectra of interfacial water [32,33], molecular ions [34], and H-bond topology [35] at water/ $\alpha$ -alumina interfaces.

The  $(1\bar{1}\bar{2}0)$  surface is significantly different from the  $(0001)$  surface. The  $(0001)$  surface is flat but the  $(1\bar{1}\bar{2}0)$  surface is rough with two exposed layers of oxygen atoms. Furthermore, at the  $(0001)$  surface, there is only one type of aluminol group,  $\text{Al}_2\text{OH}$ , but three types,  $\text{AlOH}$ ,  $\text{Al}_2\text{OH}$ , and  $\text{Al}_3\text{OH}$ , at the  $(1\bar{1}\bar{2}0)$  surface. There are two layers of aluminol oxygen groups at the  $(1\bar{1}\bar{2}0)$  surface. The outer layer contains  $\text{AlOH}$  and half of  $\text{Al}_2\text{OH}$  (Fig. 1). The  $\text{pK}_a$  of different types of aluminol groups are also different [36].

Although previous works reveal much useful information about the interaction between water and alumina surfaces, several issues are still not clearly resolved. For example, a quantitative description of water wetting at alumina surfaces, or the behavior of water H-bonded with different types of aluminol groups, is still lacking. A

powerful tool to study water wetting near solid surfaces is to measure the contact angle (CA), which has been extensively used to understand the interaction between waters and a variety of surfaces [37–40]. However, the experimentally measured contact angles are divergent with themselves [41,42]. When it comes to superhydrophilic surfaces, which can be completely wetted by water with contact angles close to  $0^\circ$ , measuring contact angles only is not enough to describe the hydrophilicity of the surfaces unless the roughness of the surfaces are modified [43].

When a water droplet is placed on the  $(0001)$  surface, complete wetting with a contact angle close to  $0^\circ$  is observed, indicating that the surface is strongly hydrophilic [30]. Our hypothesis is that the driving force of such high hydrophilicity comes from strong H-bonds that waters donate to the surface, because such H-bond modes are observed at the  $\alpha$ -alumina( $0001$ ) interfaces but not the  $\alpha$ -quartz( $0001$ ) surface, a moderately hydrophilic surface [44].

To improve the understanding of water/ $\alpha$ -alumina interfaces, especially the microscopic pictures of water wetting, we carried out classical MD simulations to study a water nano-droplet in contact with the  $\alpha$ -alumina  $(0001)$  and  $(1\bar{1}\bar{2}0)$  surfaces, revealing that both surfaces are superhydrophilic, based on the simulated contact angles and water density fluctuations. The comparison of free energies to remove interfacial water indicates that the  $(0001)$  surface is more hydrophilic than the  $(1\bar{1}\bar{2}0)$  surface at the nanoscale. The reason for the superhydrophilic character is the strong H-bonds that water molecules donate to aluminols. Interestingly, the strengths of the H-bonds are asymmetric: aluminols donate weak H-bonds to water. The interactions between water and aluminols induce patterning of interfacial waters, which are localized and oriented according to the underlying alumina crystal lattice. Our results show that the superhydrophilicity of alumina surfaces is due to strong H-bonds that waters donate to aluminol groups and highlight how MD simulations can be used to interpret macroscopic behavior of interfacial water using microscopic structures.

## 2. Simulation setup and contact angle measurements

The atomic configurations of  $\alpha$ -alumina surfaces were taken from Lutterotti's work [45] and the surface is fully hydroxylated

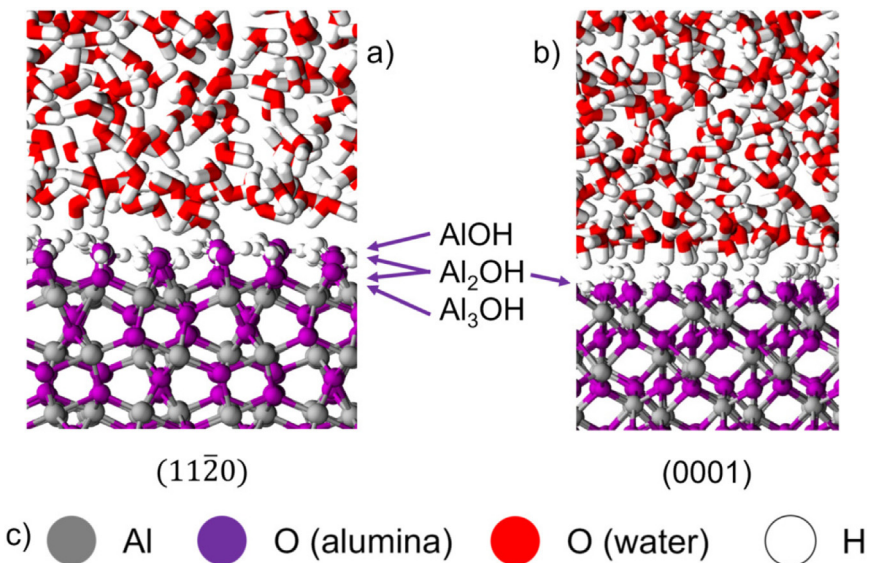


**Fig. 1.** Snapshots of MD simulation configurations of the two interfaces. (a) Atomic configurations of the water/alumina( $1\bar{1}\bar{2}0$ ) interface, there are three types of aluminol groups located at different positions. (b) At the  $(0001)$  surface, there is only one type of aluminol group and they are all anchored on the same plane. (c) Color scheme: grey: aluminum, purple: surface oxygen, red: water oxygen, white: hydrogen. (For interpretation of the references to colour in this figure legend, the reader is referred to the web version of this article.)

based on previous results [46,47]. All classical MD simulations were carried out using GROMACS 2016.3 [48–54]. No alumina atoms were fixed so they are mobile. All simulations were performed using the  $NP_{XY}L_Z$  ensemble, where constant pressure, 1 bar, was maintained on the X and Y directions using the Parrinello-Rahman barostat [55,56] and the length in the Z direction was fixed as 40 nm. The simulations contained  $8 \times 8$  or  $8 \times 6$  unit cells, resulting in the average size of the  $L_X = 3.8$  nm or 4.2 nm and  $L_Y = 3.3$  nm or 4.7 nm, for the (0001) and (11̄20) surfaces, respectively. The thicknesses of the alumina (0001) and (11̄20) solid were about 1 and 4 nm, respectively. The temperature in all simulations was maintained at 300 K using the Nosé-Hoover thermostat with a relaxation time of 0.1 ps [57,58]. The number of water molecules was about 10000 and two water/vacuum interfaces were set to maintain the pressure of water–vapor coexistence in the Z direction (Fig. S1) on both sides in simulations. Water bonds were fixed during the simulations using the LINCS algorithm [59]. The short-range interactions were neglected beyond 1 nm and long-range electrostatic interactions were calculated using particle-mesh Ewald summations [60]. Periodic boundary conditions are applied on all X, Y and Z directions.

The ClayFF force field [61] and SPC/E water model [62] were applied to describe the alumina surfaces and water, respectively. In previous MD simulations, the ClayFF force field reproduces the density distribution of interfacial water at the alumina (0001) surface, comparing to ab initio MD simulations and X-ray reflectivity spectra [24]. ClayFF also reproduces the distribution of orientations of surface OH groups and ion adsorption comparing to AIMD and experimental measurements [24]. The ClayFF force field has been applied to study a variety of interfacial phenomena at water/alumina surfaces [13,63,15].

When calculating the free energy for water removal, umbrella sampling was applied using the PLUMED package v2.3.2 [64,65]. The free energy was reconstructed using the UWHAM package [66]. The number of water molecules in the target region,  $N$ , was selected as the collective variable and the kernel bandwidth  $\sigma = 0.002$  nm [67,68]. The size of the target cubic region is shown in Table 1, whose  $\langle N \rangle = 8$  were the same for all simulations. A biased potential was added during the simulations using umbrella sampling:

$$V(N) = \frac{k}{2}(N - N_0)^2 \quad (1)$$

where  $k = 0.9$  kJ/mol and  $N_0$  ranges from –14 to 14 in each window.

To calculate contact angles, a new series of simulations containing a hemispherical water droplet with 1000 water molecules on alumina surfaces was carried out. The simulation box was extended to allow the water droplet to spread:  $32 \times 32$  unit cells or about  $15.76$  nm  $\times$   $13.65$  nm for the (0001) surface and  $32 \times 24$  unit cells or  $16.94$  nm  $\times$   $17.24$  nm for the (11̄20) surface. For each surface, three independent simulations were carried out. The wetting dynamics was characterized using the shape of a water droplet on the top of the alumina surfaces. Water oxygen atoms were projected onto the surface forming a circle and then

its radius was fitted. Instead of reporting the time-series contact angles, the relative radii were plotted (Fig. 3) because it is easier to measure when water molecules spread into a thin layer.

To measure the contact angle,  $\alpha$ -alumina prisms (Egorov Scientific) were cleaned as follows. First,  $\alpha$ -alumina prisms were soaked in acetone (Fisher Chemical) for 15 min then sonicated in 18 MΩ·cm deionized (DI) water for 30 min. Next, prisms were immersed in piranha solution,  $H_2SO_4+H_2O_2$  (J.T. Baker, Avantor Performance Materials, LLC) 3:1, (caution! Piranha solution is a strong oxidizing agent which reacts violently with most organic materials and must be handled with extreme care) at 80 °C for 30 min, then rinsed with DI water and blown dry by ultra-pure  $N_2$  gas ( $\geq 99.99\%$ ). After the wet cleaning step, prisms were sealed in the chamber of a HARRICK PDC-32G plasma cleaner and treated with radiofrequency plasma and UV irradiation for 2 min prior to the contact angle measurement. Water contact angles on  $\alpha$ -alumina prisms were measured by the sessile drop method: 5  $\mu L$  of DI water was added onto the polished flat  $\alpha$ -alumina surfaces (15 mm  $\times$  15 mm) and the tangent angle formed at the air, water, and sapphire interface was calculated using the ImageJ software [39]. Contact angle measurements of water on  $\alpha$ -alumina (0001) and (11̄20) surfaces were repeated 14 and 12 times, respectively; each contact angle measurement was performed after the complete cleaning protocol. Besides the surface cleaning method described above, separate organic solvent cleaning and piranha cleaning followed by plasma and UV treatments were done to test the effects of surface cleanliness to contact angle results.

### 3. Results

#### 3.1. Hydrophilic character of alumina surfaces

The contact angle of water on the  $\alpha$ -alumina (11̄20) surface is  $3.1 \pm 0.7^\circ$ , while on the (0001) surface it is  $2.7 \pm 0.7^\circ$  (Fig. 2), implying that both surfaces are strongly hydrophilic after the completed cleaning process. Since the standard deviations are larger than the differences between the averages, the water contact angles on both surfaces can be considered as the same. The results are in good agreement with previous results that the water contact angle on the  $\alpha$ -alumina (0001) surface is less than  $5^\circ$  [41]. However, contact angle measurements of water for other crystal faces of  $\alpha$ -alumina have not been reported.

Surface cleaning is critical. XPS and AFM analyses show that trace amounts of contaminants can alter the inherent properties of the surface and change the value of contact angle. The  $\alpha$ -alumina prisms cleaned only by organic solvents such as ethanol, isopropanol, or acetone for 12 h left an average of 13–17% carbon atomic residues, while producing water contact angles  $> 36^\circ$  [42,41,69]. The  $\alpha$ -alumina prism cleaned by freshly prepared piranha for 20 min left  $10 \pm 1\%$  of carbon atomic residues and generated a water contact angle of  $8 \pm 2^\circ$  [42,41,69]. At ambient conditions, the organic residues on alumina surface gets hydroxylated forming hydrocarbon which increases the degree of contact angle [70,71]. In this work, the  $\alpha$ -alumina substrates were cleaned by acetone, piranha, plasma and UV light to minimize the organic residues that remained, resulting in small contact angles.

Contact angles observed in MD simulations are consistent with experimental measurements. The hemispherical water droplet spreads to a thin water layer, covering the alumina surfaces after 3 ns (Fig. 3), indicating fast and complete wetting of both surfaces, consistent with a previous result [15]. MD simulations using another force field predict a contact angle of  $90^\circ$  at the alumina (0001) surface, in stark contradiction to our experimental and computational results [72]. Although the contact angles of nanoscale water droplets are not quantitatively calculated in this work,

Table 1

The size of the target region in umbrella sampling simulations for water removal.

System	X & Y	Z
alumina (0001)	1.000 nm	0.333 nm
alumina (11̄20)	0.941 nm	0.442 nm
bulk	1.000 nm	0.247 nm

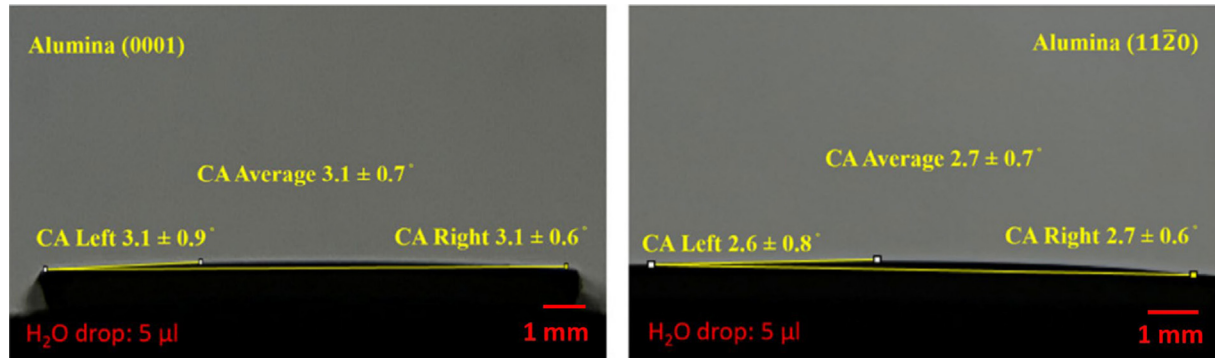


**Fig. 2.** Water spreading on the alumina surfaces. A drop of deionized water on the alumina (0001) surface (left) and the alumina (11-20) surface (right). The water contact angle was calculated as described in the text using the yellow lines added by ImageJ software.

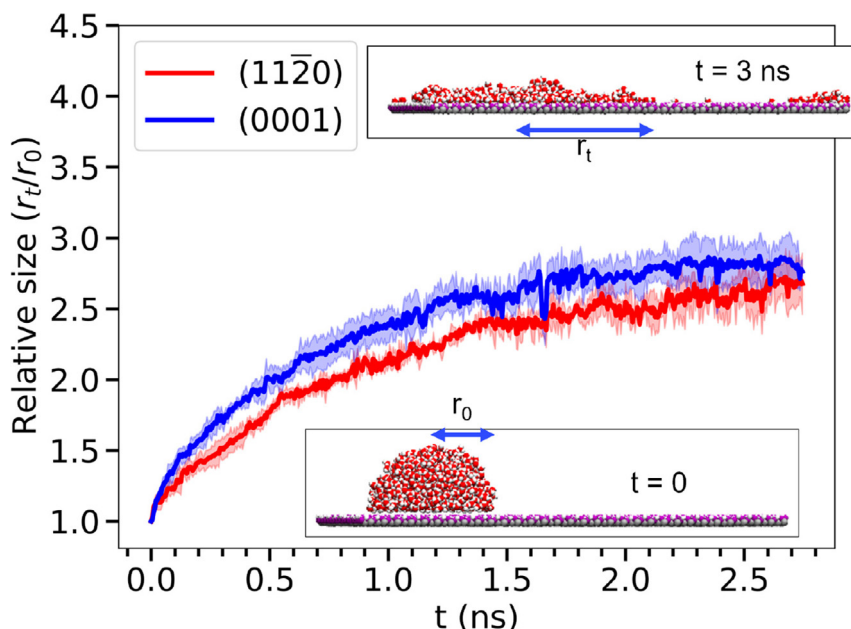


**Fig. 3.** Wetting dynamics of a water droplet on the alumina (0001) and (11-20) surfaces. Two insets represent the initial (bottom,  $t = 0$ ) and final states (top,  $t = 3$  ns) of one of three simulations using the (11-20) surface. The shape of the water droplet on the (0001) surface is similar. Only one layer of alumina atoms is shown for clarity.  $r_0$  and  $r_t$  are the radius of the water droplet projected to the surface at  $t = 0$  and time  $t$ , respectively. The shading represents the standard deviation of three independent simulations at each  $t$ . After 3 ns, the water droplet spreads into a thin layer covering the alumina (11-20) surface (top) and the contact angle is close to 0°.

the trajectories show that they are close to 0°. This could be the evidence that both surfaces are strongly hydrophilic. At the (0001) surface, the water droplet spreads slightly faster than at the (11-20) surface. However, it is difficult to compare their hydrophilicity when both surfaces are completely wetting and their water contact angles are zero.

An alternative way to determine the interaction between surfaces and water is to measure the density fluctuations of interfacial water and the associated cost of displacing water from a specified volume near the surface [73–75]. The work required to displace water from the interface can be related to the interfacial tension, such that surfaces requiring more work to displace interfacial water are more hydrophilic. In detail, after removing water molecules from a water/alumina interface, a cavity is created delimited by an air/alumina and a water/air interface with cross-sectional surface area  $A$  (Fig. 4c). The same protocol is applied to bulk water to create two water/air interfaces (Fig. 4b). Since forming these cavities in water is a rare event, indirect umbrella sampling (INDUS) is used to bias the simulations [68,67]. The free energy

to create such cavities at the water/alumina interfaces ( $\Delta G_{\text{surface}}$ ) and in the bulk ( $\Delta G_{\text{bulk}}$ ) is calculated as the difference in the potential of the mean force:

$$\Delta G_{\text{surface}} = G_{\text{surface}}(0) - G_{\text{surface}}(\langle N \rangle) \quad (2)$$

$$\Delta G_{\text{bulk}} = G_{\text{bulk}}(0) - G_{\text{bulk}}(\langle N \rangle) \quad (3)$$

where  $G_{\text{region}}(N)$  is the free energy when  $N$  water molecules are in the region of interest [74].

For macroscopic volumes, the free energies  $\Delta G_{\text{surface}}$  and  $\Delta G_{\text{bulk}}$  can be related to the surface tensions of the corresponding solid–gas ( $\gamma_{SG}$ ), liquid–gas ( $\gamma_{LG}$ ), and solid–liquid interfaces ( $\gamma_{SL}$ ). Ignoring contributions from the sides of the cuboidal volumes, which are independent of the volume's location, the free energy change upon emptying the volume near the solid surface is

$$\Delta G_{\text{surface}} = (\gamma_{SG} + \gamma_{LG} - \gamma_{SL})A, \quad (4)$$

and the analogous free energy difference in the bulk is

$$\Delta G_{\text{bulk}} = 2\gamma_{LG}A. \quad (5)$$

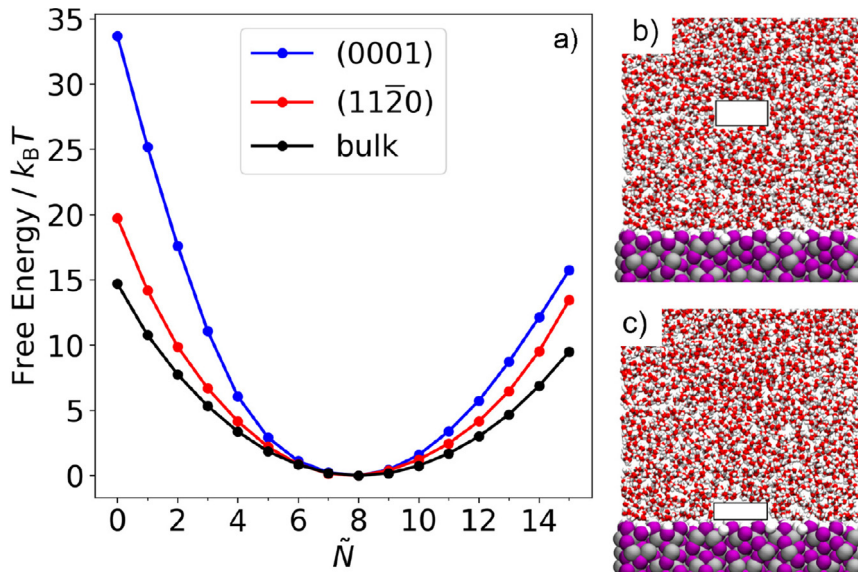


**Fig. 4.** Results and simulation settings to calculate the density fluctuations of interfacial water. (a) The potential of the mean force as a function of the number of water molecules ( $N$ ) inside the target region. ( $N=8$  in simulations of this work. (b) and (c) Snapshots of biased simulations containing no water molecules in target regions. The target region is in bulk water (b) or at the surface (c). The dimensions of the empty regions are described in Table 1.

Then, by using Young's Equation,  $\gamma_{SG} = \gamma_{SL} + \gamma_{LG} \cos \theta_c$ , the contact angle,  $\theta_c$ , can be predicted from the difference between  $\Delta G_{\text{surface}}$  and  $\Delta G_{\text{bulk}}$ ,

$$\cos \theta_c = \frac{\Delta G_{\text{surface}} - \Delta G_{\text{bulk}}}{\gamma_{LG} A} + 1. \quad (6)$$

Indeed, previous work has shown that Eq. 6 can be successfully applied to wetting on a series of self-assembled monolayer surfaces when using a size-dependent surface tension in place of the macroscopic  $\gamma_{LG}$  [76].

The alumina (0001) and (11-20) surfaces are both completely wetting,  $\cos \theta_c = 1$ , and Eq. 6 predicts that  $\Delta G_{\text{surface}} = \Delta G_{\text{bulk}}$  at the macroscale. However, the simulation results in Fig. 4 show that this is not the case at the nanoscale. Instead, both  $\Delta G_{(0001)}$  and  $\Delta G_{(11-20)}$  are larger than  $\Delta G_{\text{bulk}}$ , and Eq. 6 unphysically predicts that  $\cos \theta_c > 1$ . This suggests that surfaces can be more hydrophilic on nanoscale lengthscales than is possible macroscopically and that this nanoscale hydrophilicity can be probed through the analysis of water density fluctuations. Our results indicate that the interactions between water and alumina are stronger than those between water molecules, suggesting that the alumina surfaces are "superhydrophilic" or "superwetting", as has also been observed for  $\text{TiO}_2$  surfaces [43]. Moreover, because  $\Delta G_{(0001)} > \Delta G_{(11-20)}$ , the (0001) surface can be considered more hydrophilic than the (11-20) surface, at least on the lengthscale of our observation volumes.

### 3.2. Interfacial water: structural aspects

To develop a microscopic picture of water/alumina interfaces, we first look at the geometry of interfacial water, such as the joint density distribution of distance ( $Z$ ) and water polar orientation ( $\theta_\mu$ ), within 1 nm from both the alumina (0001) and (11-20) (Fig. 5h and e) surfaces, marked as  $P(Z, \theta_\mu)$ .  $Z = 0$  is defined as the average  $z$  coordinates of outer aluminal oxygen atoms of a surface.  $\theta_\mu$  is the angle between the opposite of water dipole moment vector and the surface normal (defined in Fig. 5a);  $0^\circ$  or  $180^\circ$  indicate that water molecules point away from or toward to the surface, respectively (Fig. 5a). Water molecules accumulate at about

0.2 nm from the (11-20) surface or 0.25 nm from the (0001) surface and interfacial water molecules form H-bonds with aluminal groups. Quantitative analysis shows that most aluminal groups on both surfaces either donate or accept H-bonds with interfacial water (Fig. S7c).

Some commonly observed binding motifs at the (11-20) surface are water donating an H-bond to  $\text{Al}_2\text{OH}$  (W- $\text{Al}_2\text{OH}$ ), donating an H-bond to  $\text{AlOH}$  (W- $\text{AlOH}$ ), or accepting an H-bond from  $\text{Al}_3\text{OH}$  (W- $\text{Al}_3\text{OH}$ ). At the (0001) surface, water molecules donate or accept H-bonds with aluminal groups, marked as W-(0001) or (0001)-W, respectively. These binding motifs also correlate with water polar orientations. At the (11-20) surface, two features appear in the density plot  $P(Z, \theta_\mu)$ : at ( $Z = 0.25$  nm,  $\theta_\mu = 135^\circ$ ), waters donate hydrogen bonds to  $\text{AlOH}$ . The wide feature at  $Z = 0.2$  with  $\theta_\mu$  ranging from  $0^\circ$  to  $100^\circ$  represents water that accepts an H-bond from  $\text{Al}_2\text{OH}$  or  $\text{Al}_3\text{OH}$ ; the wide range of angles spanned by these H-bonds is consistent with the delocalized nature of the charge density of the water oxygen site [77]. Notice that oxygen atoms on  $\text{Al}_3\text{OH}$  have 4 tetrahedral covalent bonds and cannot accept H-bonds from water. Water H-bonds at the (0001) interface are much simpler: water can point toward to the surface, donating H-bonds ( $Z = 0.25$  nm,  $\theta_\mu = 130^\circ$ ) or point away from the surface, accepting H-bonds ( $Z = 0.25$  nm,  $\theta_\mu = 10^\circ$ ), as described previously [24].

To understand how interfacial water molecules interact with alumina surfaces, the water in-plane densities at the interfacial region were calculated using the position of water oxygen atoms (Fig. 6). The interfacial region ends at the first minimum in the density profile (Fig. S2), i.e.  $Z = 0.3515$  nm for the (11-20) interface and  $Z = 0.3405$  nm for the (0001) interface. Interfacial waters are not randomly distributed at alumina surfaces; instead, the water adsorption pattern follows the atom configuration of the unit cell of alumina surfaces. (Fig. 6a, b).

On the (11-20) surface, the water density near oxygen atoms is much higher than that at other regions, especially near the  $\text{Al}_3\text{OH}$  groups. Two reasons are proposed for such observations. First, the mobility of aluminal groups on the  $\text{Al}_3\text{OH}$  is different from others since these surface oxygen atoms are bonded with 4 atoms and those aluminal groups can not rotate. The orientations of  $\text{Al}_3\text{OH}$  are limited and perpendicular to the surface (Fig. S7b). Second,

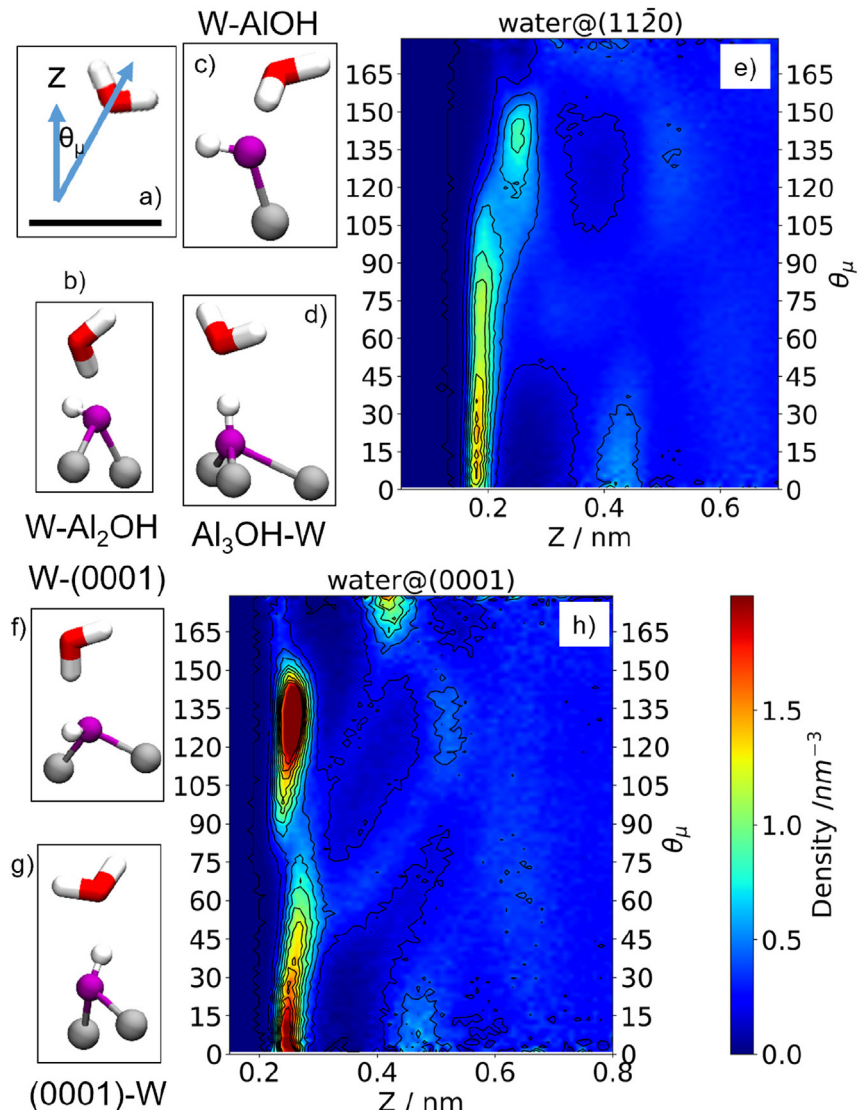


**Fig. 5.** Distributions of  $P(Z, \theta_\mu)$  and typical H-bond structures. (a) Schematic illustrating of the definition of water polar orientations.  $\theta_\mu$  is the angle between the opposite of the water dipole and the surface normal. (b), (c) and (d) snapshots of typical H-bonding motifs between water and alumina surfaces, including W-Al<sub>2</sub>OH, W-AlOH and Al<sub>3</sub>OH-W, respectively. (e) Distribution of  $P(Z, \theta_\mu)$ , where  $Z$  is the distance between water oxygen and surface oxygen atoms. (b)-(e) are calculated from simulations with the (1120) surface. (f) and (g) snapshots of H-bond modes W-(0001) and (0001)-W. (h) Distribution of  $P(Z, \theta_\mu)$  at the (0001) surface, reprinted with permission from Ref. [24]. Copyright (2019) American Chemical Society. The color bar is for both (e) and (h). (For interpretation of the references to colour in this figure legend, the reader is referred to the web version of this article.)

the (11-20) surface is not flat and the position of Al<sub>3</sub>OH groups is lower, forming a concave site that stabilizes adsorbed water. Another site with high local water density is the lower Al<sub>2</sub>OH. It is worth mentioning that the thickness of the water slab at different sites are different: Al<sub>3</sub>OH is buried but AlOH is the outermost aluminol.

On the (0001) surface, water molecules accumulate at triangular sites defined by three aluminol oxygen atoms with a center aluminol atom. Interestingly, the orientations of the aluminol OH vectors are counterclockwise (Fig. 6b) and interfacial waters have higher density in the opposite direction of the OH vector of the aluminol groups. In addition, previous simulations have shown that the triangular sites also have strong affinity to sodium and halide ions [24]. The specific pattern of water adsorption at the surfaces indicates their strong interaction and is consistent with the observation that both surfaces are superhydrophilic.

### 3.3. Interfacial water: hydrogen bond dynamics

Strong interactions between interfacial water and alumina surfaces affect the properties of H-bonds, including their lifetimes, which can be described using the continuous H-bond lifetime autocorrelation function,  $S(t)$ , defined as

$$S(t) = \frac{\langle A(0)A(t)s(t) \rangle}{\langle A(0)A(0) \rangle}, \quad (7)$$

where

$$s(t) = \prod_{i=0}^t A(i), \quad (8)$$

$A(t)=1$  if two water molecules are H-bonded at time  $t$  and  $A(t)=0$  if not;  $s(t)=1$  if an H-bond remains unbroken and  $s(t)=0$  if it has been broken at least once. The criterion of an H-bond is based on the geometry of the donor and acceptor proposed by Luzar and Chan-

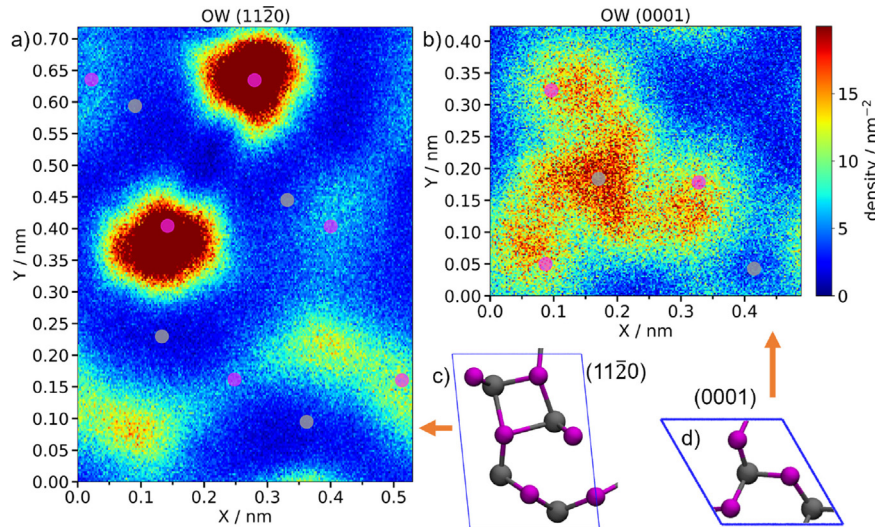


**Fig. 6.** Interfacial water oxygen 2D density profiles parallel to the  $(11\bar{2}0)$  and  $(0001)$  surfaces; the color bar shows the density for both plots. Purple dots and gray dots on these plots are the positions of oxygen and aluminum atoms in this unit cell. Although unit cells of both alumina surfaces are monoclinic so their shapes are not rectangular, densities were plotted in rectangles following the periodic boundary condition. (a) The  $(0001)$  interface, (b) The  $(11\bar{2}0)$  interface. (c), (d) Atom configurations of a unit cell of the  $(11\bar{2}0)$  or  $(0001)$  surfaces. Hydrogen atoms are not shown and the blue lines are the boundary of a unit cell. (For interpretation of the references to colour in this figure legend, the reader is referred to the web version of this article.)

dler; [78] an H-bond exists if the distance between donor oxygen  $O_d$  and acceptor oxygen  $O_a$  is less than  $3.5 \text{ \AA}$  and the O-O-H angle,  $\angle O_a O_d H_d$ , is less than  $30^\circ$ . Continuous autocorrelation functions describe how long an H-bond survives [79].

H-bond lifetimes depend on the type of aluminol group (Fig. 7). Overall,  $S(t)$  follows an approximately exponential decay. Among all H-bonding motifs,  $\text{Al}_3\text{OH-W}$  has the longest H-bond lifetime, which may be the result of the limited motions of  $\text{Al}_3\text{OH}$ .  $\text{W-Al}_3\text{OH}$  is not shown because it is difficult for  $\text{Al}_3\text{OH}$  groups to accept an H-bond. Except for  $\text{Al}_3\text{OH-W}$ ,  $\text{W-(0001)}$  has a distinguishable longer lifetime than other H-bonding motifs, including those in bulk water; the lifetime of  $(0001)\text{-W}$  is also longer than

$\text{AlOH-W}$  or  $\text{Al}_2\text{OH-W}$ . Based on the population of aluminol types, we find that the overall H-bond lifetime at the  $(0001)$  surface is slightly longer than at the  $(11\bar{2}0)$  surface (details discussed in the SI).

H-bonds between interfacial water and surfaces are asymmetric with respect to donors and acceptors. The lifetime of W-surface H-bonds is longer than that of surface-W H-bonds for the same type of aluminol groups. On the  $(11\bar{2}0)$  surface, the H-bond lifetimes follow this trend:  $\text{W-AlOH} > \text{AlOH-W}$  and  $\text{W-Al}_2\text{OH} > \text{Al}_2\text{OH-W}$ ; on the  $(0001)$  surface:  $\text{W-(0001)} > (0001)\text{-W}$ , as shown in Fig. 7. Our hypothesis is that the strength of H-bonds is consistent with

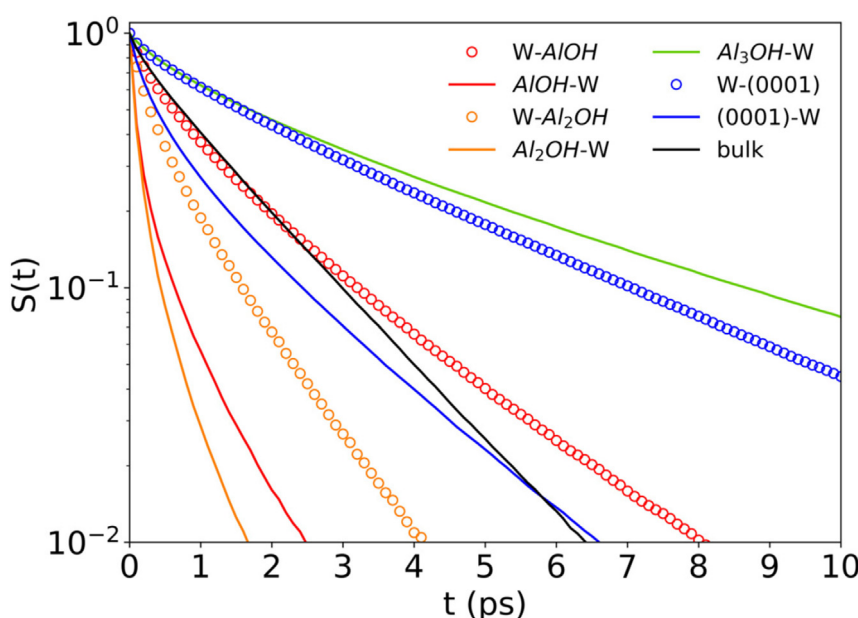


**Fig. 7.** H-bond lifetime autocorrelation functions defined in Eq. 7. W-surface and surface-W H-bonds are plotted with circle symbols or lines, respectively. Different colors represent the type of aluminol groups in the H-bonds: blue: aluminol groups of the  $(0001)$  surface, red:  $\text{AlOH}$ , orange:  $\text{Al}_2\text{OH}$ , green:  $\text{Al}_3\text{OH}$ . The last three are for the  $(11\bar{2}0)$  surface. All W-surface H-bonds (circles) show longer lifetime than surface-W H-bonds (lines with the same color), except for  $\text{Al}_3\text{OH}$ . (For interpretation of the references to colour in this figure legend, the reader is referred to the web version of this article.)

their lifetime: W-surface H-bonds are stronger than surface-W ones.

The strength of an H-bond is correlated with the geometry [80]. Though a simple examination of the geometry of H-bond structures cannot provide quantitative H-bond strengths, qualitative comparison can still be made [80]. Generally, H-bonds with shorter  $O_dO_a$  distance and smaller  $\angle O_aO_dH_d$  (left bottom corner) are qualitatively stronger than the opposite (Fig. 8j). First, by comparing W-surface and surface-W H-bonds, we found that H-bond strength is asymmetric, W-surface H-bonds are stronger than that in bulk water since their average  $O_dO_a$  distance is slightly shorter than in the bulk, but surface-W H-bonds are significantly weaker than those in bulk. Except for the  $Al_3OH$  groups, plots of probability distribution of H-bonds show that H-bonds of W-surface are short and more linear than those of W-surface H-bonds (Fig. 8 ab, cd and gh). At the (0001) interface, the average donor–acceptor distance of W-(0001) H-bonds is shorter than at the (11̄20) surface. The strong W-surface H-bonds are important for the hydrophilicity of surfaces and the asymmetric H-bonds, especially the weak surface-W H-bonds, result in the high frequency aluminol vibrations observed in vSFG spectra [81,33,44,82].

### 3.4. Water translational and rotational dynamics

Several dynamical properties of interfacial water are calculated and compared with bulk water. As discussed below, simulation results show that dynamics of interfacial water molecules are slowed down by alumina surfaces because of strong interactions between water and hydrophilic alumina surfaces.

First, the 2D mean square displacement (MSD) of water oxygen atoms was calculated using:

$$MSD_{2D}(t) = \left\langle \left( |x(t) - x(0)|^2 + |y(t) - y(0)|^2 \right) s_r(t) \right\rangle \quad (9)$$

which can be used to describe the in-plane translation of water molecules at the interfacial region. High MSD values indicate fast motion of water molecules. Water molecules in the bulk travel about 4 times as fast as interfacial water (Fig. 9a), consistent with the hydrophilicity and strong interactions between interfacial water and surfaces. The parallel diffusion of water shows no distinguishable difference between the two surfaces though the (0001) surface is more hydrophilic.

Another behavior investigated is the water residence time evaluated via the following autocorrelation function:

$$R(t) = \frac{\langle r(0)r(t)s_r(t) \rangle}{\langle r(0)r(0) \rangle} \quad (10)$$

$$s_r(t) = \prod_{i=0}^t R(i) \quad (11)$$

The residence time correlation function,  $R(t)$ , is used to describe how long a water molecule stays in a certain region; in this work the continuous autocorrelation function is reported, that is, once a water molecule leaves the specified region, its contribution to the correlation function is zero. A slower decay of  $R(t)$  indicates a longer residence time at the interface and hence slow perpendicular translations.  $R(t)$  is quasi-log-linear for all three environments, similar to the behavior of water H-bond lifetimes Fig. 9b. The residence time of interfacial water is much longer than that of bulk water, indicating that alumina surfaces slow down water translation perpendicular to the interfaces.

Lastly, water reorientation autocorrelation functions were calculated:[83]

$$C_n(t) = \frac{\langle P_n(\mu_{OH}(t)\mu_{OH}(0)s_r(t)) \rangle}{\langle P_n(\mu_{OH}(0)\mu_{OH}(0)) \rangle}, \quad (12)$$

where  $P_n$  is the  $n^{\text{th}}$  order Legendre polynomial, and we consider the first and second order polynomials,

$$P_1(x) = x \quad (13)$$

$$P_2(x) = \frac{1}{2}(3x^2 - 1) \quad (14)$$

Both the 1st and 2nd order autocorrelation functions in Fig. 9c show the reorientation relaxation times of water molecules follow this trend:  $\tau_{(0001)} > \tau_{(11\bar{2}0)} > \tau_{\text{bulk}}$ , which is consistent with the hydrophilicity comparison predicted by water density fluctuations discussed above. This is also consistent with previous work identifying correlations between rotational dynamics and surface hydrophilicity [84–86]. Unlike the translation of water molecules at the interface, there is a significant difference in the reorientation dynamics for the (0001) and (11̄20) interfaces, consistent with the

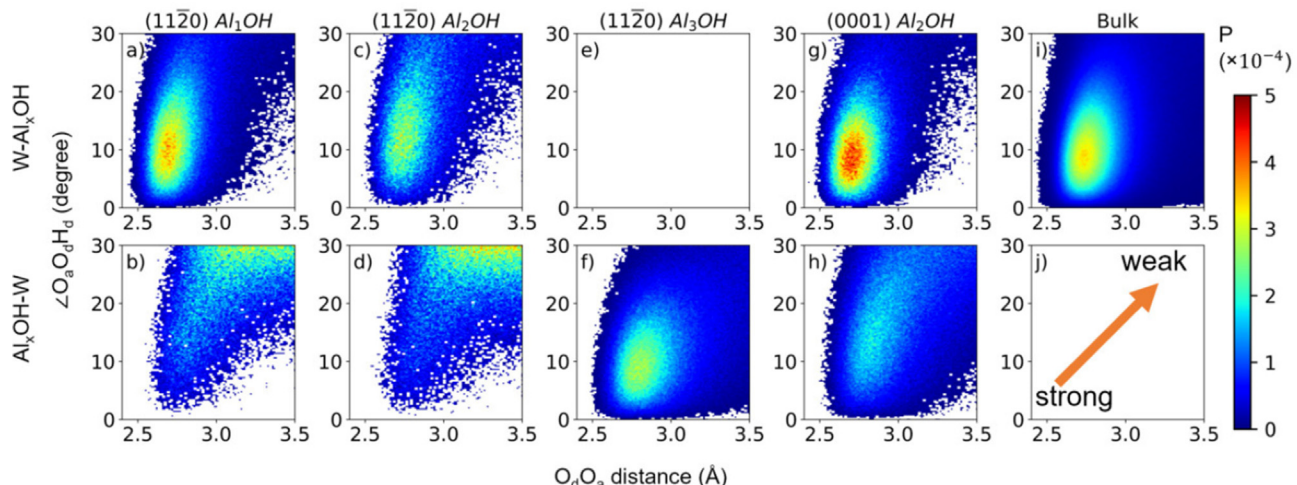


**Fig. 8.** Normalized probability distributions of H-bond geometry based on H-bond motifs. (a) W-AlOH, (b) AlOH-W, (c) W-Al<sub>2</sub>OH, (d) Al<sub>2</sub>OH-W, (e) W-Al<sub>3</sub>OH, which is rare in simulations so most points are 0, (f) Al<sub>3</sub>OH-W, (g) W-(0001), (h) (0001)-W, (i) bulk water. In plots (a)–(h), the top and bottom rows represent water-to-surface and surface-to-water H-bonds, respectively. (j) The left bottom corner represents strong H-bonds with short distance and linear geometry; the right top corner represents the opposite. The color bar is for plots (a)–(i).

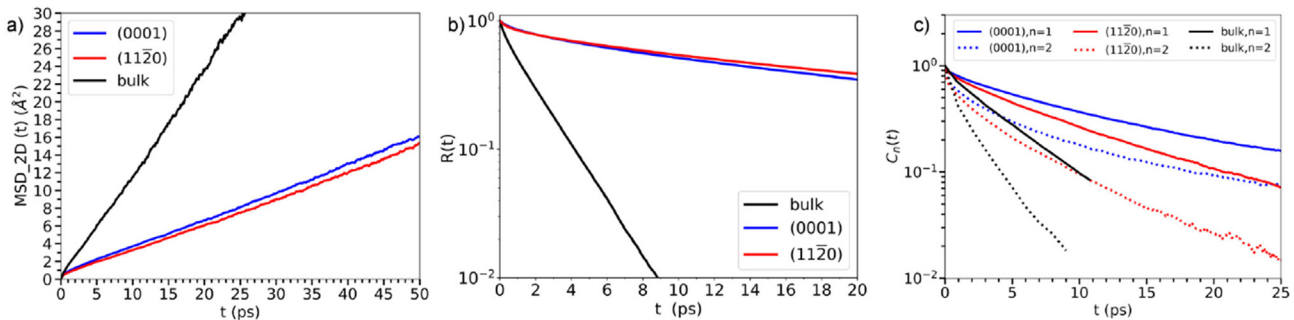


**Fig. 9.** Water dynamics at alumina interfaces or in the bulk. (a) 2D in-plane water mean square displacement versus time, defined by Eq. 9. (b) water residence time autocorrelation function, defined by Eq. 10. (c) water reorientation time correlation function, defined by Eq. 12. In figure (c), the autocorrelation function of bulk water is replotted from previous work [87]. In all plots, bulk, the (11-20) and (0001) surfaces are plotted in black, red and blue respectively.

fact that the (0001) surface is more hydrophilic as demonstrated through probing water density fluctuations.

#### 4. Discussion

There are no aluminol groups on as-cleaved alumina surfaces. However, when contacting water, dissociative adsorption takes place on the surface, creating aluminol groups [46]. The number density of aluminol OH groups on the alumina (0001) and (11-20) surface are 15.3 OH/nm<sup>2</sup> and 16.8 OH/nm<sup>2</sup> (experimental value) [45], or 14.3 OH/nm<sup>2</sup> and 15.7 OH/nm<sup>2</sup> (simulations in this work). If bulk water is cut to form a water slab, there could be a maximum of 11.7 water molecules forming hydrogen bonds per 1 nm<sup>2</sup>, given the distance cut-off for a hydrogen bond of 3.5 Å. Compared to bulk water, the density of OH groups at the alumina (0001) and (11-20) surfaces is higher, which could be one reason for their superhydrophilicity [88]. Similar trends can be found at other surfaces, for example, the OH density at a moderate hydrophilic surface, fused silica, is 3.5 OH/nm<sup>2</sup>, much lower than alumina [35]. However, the hydrophilicity of a surface cannot be simply determined by the number density of OH groups on the surface. The (11-20) surface has higher number density of OH groups but less hydrophilicity according to our simulations. Other factors that affect water wetting cannot be overlooked when predicting interactions between water and solid surfaces.

An important factor to determine the hydrophilicity of surfaces is the pattern of hydrophilic groups. The hydrophilicity of an interface is “context-dependent and nonadditive” [89], indicating that local structures of a surface cannot be neglected. Instead of carrying out MD simulations with biased sampling of all water interfaces, one possible solution could be developing simplified descriptors that can be used by machine learning based techniques to map the pattern and hydrophilicity [90]. As for this work, the (0001) surface has a perfect triangular pattern but the pattern on the (11-20) surface is irregular. What is more, compared to the flat (0001) surface, the (11-20) surface is rougher. Our hypothesis is that a well-ordered pattern commensurate with water’s H-bonds, like the (0001) surface, could align the network of interfacial water, whereas the more irregular (11-20) surface cannot. However, predicting the hydrophilicity from the pattern of surfaces is not a trivial problem. The lower hydrophilicity of the (11-20) surface may also be due to its roughness at the nanoscale; in general, rough surfaces have a higher contact angles.

Simulations in this work are based on classical MD using the ClayFF force field, which assigns -0.95e to all oxygen atoms of aluminol groups and very similar charges to both water and aluminol hydrogen atoms. Compared to -0.8476e of a water oxygen in the

SPC/E model, an aluminol oxygen atom contains more negative charge, though the whole surfaces are neutral, containing no net charge. Thus it is not surprising that interfacial waters donate strong H-bonds to the more negative aluminol oxygen and cannot accept stronger H-bonds with short donor-acceptor distance because of the repulsion between oxygen atoms of the donor and acceptor.

In this work, we observed different H-bond strengths between interfacial water and different aluminol groups. This behavior may be related to the different pK<sub>a</sub> values of aluminol groups. At the alumina (0001) surface, there are two pK<sub>a</sub> values corresponding to the protonation states:



These pK<sub>a</sub> have been calculated in previous ab initio MD simulations on the gibbsite (0001) surface: pK<sub>a1</sub> = 1.3 and pK<sub>a2</sub> = 22.0, indicating strong affinity for protons and making the surface only donate weak H-bonds [91]. There are no simulated pK<sub>a</sub> at the (11-20) surface reported but experimentally estimated pK<sub>a</sub>s for Al<sub>2</sub>-OH (pK<sub>a</sub>=12.5) and Al<sub>3</sub>OH (pK<sub>a</sub><3) are divergent [36]. As a result, modeling these differences relies on additional simulations to predict H-bond behaviors. Since measuring surface pK<sub>a</sub> is challenging in experiments and there are still discrepancies between results from different techniques, investigating the correlation between surface pK<sub>a</sub> and wetting is one future direction that could yield useful insights.

In experiments, organic residues can substantially alter the surface properties and increase contact angle of water on  $\alpha$ -alumina surfaces. Using the more complete surface cleaning method contact angle of water are  $2.7 \pm 0.7^\circ$  on the (11-20) surface and  $3.1 \pm 0.7^\circ$  on the (0001) surface, which agrees with the simulations results that both types of  $\alpha$ -alumina surfaces are strongly hydrophilic. Although minimizing the effects of contamination is a challenge in contact angle measurements, it can be easily overcome in MD simulations.

#### 5. Conclusions

We investigated wetting at the water/ $\alpha$ -alumina (0001) and (11-20) interfaces using classical MD simulations and contact angle measurements. The simulation results, including fast wetting dynamics, contact angles of zero, and small density fluctuations of interfacial water, indicate that both surfaces are superhydrophilic and completely wetting. Furthermore, the free energy of interfacial water removal calculations show that the (0001) sur-

face is more hydrophilic than the (11 $\bar{2}$ 0) one. Interactions between water and surfaces promote interfacial water adsorption at specific sites, leading to ordered water structures on alumina surfaces. Translational and rotational dynamics of interfacial water are slower than for bulk water.

The superhydrophilicity of alumina surfaces are attributed to strong H-bonds, which have shorter oxygen–oxygen distances and smaller O–O–H angles ( $\angle O_a O_d H_d$ ) as well as longer lifetimes. Such a correlation between surface wetting and interfacial H-bonds is helpful to understand the properties of the interface. We also observe asymmetric H-bonds: the strength of water-to-aluminol H-bonds is significantly greater than aluminol-to-water ones. Using the density fluctuation method to calculate the work required to remove a nanoscale volume of water from the interface, we found that the alumina(0001) surface is more hydrophilic than the (11 $\bar{2}$ 0) one on the nanoscale, which cannot be determined from the almost identical contact angles [30].

There are several advantages of MD simulations when investigating wetting at solid surfaces. First, contact angles observed in MD simulations and experimental measurements are consistent, showing the accuracy of MD simulations, contradicting previous observations that contact angle at alumina surfaces are about 60°[69,71,42], due to surface contamination [41]. Such contamination can be removed by careful cleaning but MD simulations can overcome it more easily. Another advantage of MD simulations when studying superhydrophilic surfaces is that, comparing experimental methods that require modifying surface roughness [43], the density fluctuation method is much more convenient [75]. In this work, the superhydrophilicity of surfaces is connected to the strength of interfacial H-bonds, which has not been well studied in previous works [30,31]. Our observation of strong H-bonds at the water/ $\alpha$ -alumina(0001) interface is consistent with previous AIMD simulations but we use a geometry criterion instead of vibrational frequency that needs higher computational cost [44]. Future work will be how impurities at interfaces, both organic and inorganic, affect wetting at such superhydrophilic surfaces [92].

## Declaration of Competing Interest

The authors declare that they have no known competing financial interests or personal relationships that could have appeared to influence the work reported in this paper.

## Acknowledgements

We thank Dr. Mark DelloStritto for useful discussions. This work was supported as part of the Center for Complex Materials from First Principles (CCM), an Energy Frontier Research Center funded by the U.S. Department of Energy, Office of Science, Basic Energy Sciences under Award #DE-SC0012575. This work was funded by the National Institutes of Health (R01GM093290, R01GM131048, S10OD020095 to V.C.), and the National Science Foundation grant IOS-1934848 to V.C.). E.B. acknowledges and thanks the National Science Foundation for its support (NSF Grant MRI 1828421). This research includes calculations carried out on HPC resources supported in part by the National Science Foundation through major research instrumentation Grant No. 1625061 and by the US Army Research Laboratory under contract number W911NF-16-2-0189. This research used resources of the National Energy Research Scientific Computing Center (NERSC), a U.S. Department of Energy Office of Science User Facility located at Lawrence Berkeley National Laboratory, operated under Contract No. DE-AC02-05CH11231.

## Appendix A. Supplementary material

Supplementary data associated with this article can be found, in the online version, at <https://doi.org/10.1016/j.jcis.2022.07.164>.

## References

- [1] M. Chen, H.-Y. Ko, R.C. Remsing, M.F. Calegari Andrade, B. Santra, Z. Sun, A. Selloni, R. Car, M.L. Klein, J.P. Perdew, X. Wu, Ab initio theory and modeling of water, *Proc. Natl. Acad. Sci. USA* (2017) 201712499.
- [2] J. Xu, M. Chen, C. Zhang, X. Wu, First-principles study of the infrared spectrum in liquid water from a systematically improved description of h-bond network, *Phys. Rev. B* 99 (2019) 205123.
- [3] O. Demerdash, L. Wang, T. Head-Gordon, Advanced models for water simulations, *Wiley Interdiscip. Rev. Comput. Mol. Sci.* 8 (1) (2018) e1355.
- [4] R. Wang, V. Carnevale, M.L. Klein, E. Borguet, First-principles calculation of water pka using the newly developed scan functional, *J. Phys. Chem. Lett.* 11 (2020) 54–59.
- [5] O. Björneholm, M.H. Hansen, A. Hodgson, L.-M. Liu, D.T. Limmer, A. Michaelides, P. Pedevilla, J. Rossmeisl, H. Shen, G. Tocci, E. Tyrode, M.-M. Walz, J. Werner, H. Bluhm, Water at interfaces, *Chem. Rev.* 116 (13) (2016) 7698–7726.
- [6] R. Wang, M.L. Klein, V. Carnevale, E. Borguet, Investigations of water/oxide interfaces by molecular dynamics simulations, *Wiley Interdiscip. Rev. Comput. Mol. Sci.* 11 (6) (2021) e1537.
- [7] X. Shen, I.C. Bourg, Molecular dynamics simulations of the colloidal interaction between smectite clay nanoparticles in liquid water, *J. Colloid Interface Sci.* 584 (2021) 610–621.
- [8] S.S. Lee, A. Koishi, I.C. Bourg, P. Fenter, Ion correlations drive charge overscreening and heterogeneous nucleation at solid-aqueous electrolyte interfaces, *Proc. Natl. Acad. Sci. USA* 118 (32) (2021), <https://doi.org/10.1073/pnas.2105154118>, e2105154118.
- [9] Q. Pang, H. DorMohammadi, O.B. Isgor, L. Árnadóttir, Thermodynamic feasibility of the four-stage chloride-induced depassivation mechanism of iron, *npj Mater. Degrad.* 4 (1) (2020) 26.
- [10] K. Leung, First principles, explicit interface studies of oxygen vacancy and chloride in alumina films for corrosion applications, *J. Electroanal. Chem.* 168 (3) (2021) 031511.
- [11] R. Rousseau, V.-A. Glezakou, A. Selloni, Theoretical insights into the surface physics and chemistry of redox-active oxides, *Nat. Rev. Mater.* 5 (6) (2020) 460–475.
- [12] A. Soni, G.N. Patey, Why  $\alpha$ -alumina is an effective ice nucleus, *J. Phys. Chem. C* 123 (43) (2019) 26424–26431.
- [13] I.-C. Yeh, J.L. Lenhart, J.A. Orlicki, B.C. Rinderspacher, Molecular dynamics simulation study of adsorption of bioinspired oligomers on alumina surfaces, *J. Phys. Chem. B* 123 (32) (2019) 7024–7035.
- [14] K. Leung, L.J. Criscenti, A.W. Knight, A.G. Ilgen, T.A. Ho, J.A. Greathouse, Concerted metal cation desorption and proton transfer on deprotonated silica surfaces, *J. Phys. Chem. Lett.* 9 (18) (2018) 5379–5385.
- [15] S. Bekele, O.G. Evans, M. Tsige, Spreading dynamics of water droplets on a completely wetting surface, *J. Phys. Chem. C* 124 (37) (2020) 20109–20115.
- [16] J. Hautman, M.L. Klein, Microscopic wetting phenomena, *Phys. Rev. Lett.* 67 (1991) 1763–1766.
- [17] J.-B. Le, X.-H. Yang, Y.-B. Zhuang, M. Jia, J. Cheng, Recent progress toward ab initio modeling of electrocatalysis, *J. Phys. Chem. Lett.* 12 (37) (2021) 8924–8931, <https://doi.org/10.1021/acs.jpclett.1c02086>.
- [18] A.C. Fogarty, E. Duboué-Dijon, F. Sterpone, J.T. Hynes, D. Laage, Biomolecular hydration dynamics: a jump model perspective, *Chem. Soc. Rev.* 42 (13) (2013) 5672–5683, <https://doi.org/10.1039/C3CS60091B>.
- [19] D. Biriukov, O. Kroutil, M. Kabeláć, M.K. Ridley, M.L. Machesky, M. Predota, Oxalic acid adsorption on rutile: Molecular dynamics and ab initio calculations, *Langmuir* 35 (24) (2019) 7617–7630, <https://doi.org/10.1021/acs.langmuir.8b03984>.
- [20] S. Vembanur, A.J. Patel, S. Sarupria, S. Garde, On the thermodynamics and kinetics of hydrophobic interactions at interfaces, *J. Phys. Chem. B* 117 (35) (2013) 10261–10270, <https://doi.org/10.1021/jp4050513>.
- [21] S. Sarupria, S. Garde, Quantifying water density fluctuations and compressibility of hydration shells of hydrophobic solutes and proteins, *Phys. Rev. Lett.* 103 (2009) 037803.
- [22] G.V. Franks, Y. Gan, Charging behavior at the alumina-water interface and implications for ceramic processing, *J. Am. Ceram. Soc.* 90 (11) (2007) 3373–3388.
- [23] K. Murata, J. Ohyama, Y. Yamamoto, S. Arai, A. Satsuma, Methane combustion over pd/Al<sub>2</sub>O<sub>3</sub> catalysts in the presence of water: Effects of pd particle size and alumina crystalline phase, *ACS Catal.* 10 (15) (2020) 8149–8156, <https://doi.org/10.1021/acscatal.0c02050>.
- [24] R. Wang, M. DelloStritto, R.C. Remsing, V. Carnevale, M.L. Klein, E. Borguet, Sodium halide adsorption and water structure at the  $\alpha$ -alumina(0001)/water interface, *J. Phys. Chem. C* 123 (25) (2019) 15618–15628.
- [25] J.G. Catalano, Weak interfacial water ordering on isostructural hematite and corundum (0 0 1) surfaces, *Geochim. Cosmochim. Acta* 75 (8) (2011) 2062–2071.
- [26] A. Tuladhar, S.M. Piontek, E. Borguet, Insights on interfacial structure, dynamics, and proton transfer from ultrafast vibrational sum frequency

generation spectroscopy of the alumina(0001)/water interface, *J. Phys. Chem. C* 121 (9) (2017) 5168–5177.

[27] A. Tuladhar, S. Dewan, J.D. Kubicki, E. Borguet, Spectroscopy and ultrafast vibrational dynamics of strongly hydrogen bonded oh species at the  $\alpha$ -Al<sub>2</sub>O<sub>3</sub> (1120)/H<sub>2</sub>O interface, *J. Phys. Chem. C* 120 (29) (2016) 16153–16161.

[28] L. Zhang, C. Tian, G.A. Waychunas, Y.R. Shen, Structures and charging of  $\alpha$ -alumina (0001)/water interfaces studied by sum-frequency vibrational spectroscopy, *J. Am. Chem. Soc.* 130 (24) (2008) 7686–7694.

[29] J. Sung, Y.R. Shen, G.A. Waychunas, The interfacial structure of water/protonated  $\alpha$ -Al<sub>2</sub>O<sub>3</sub> (1120) as a function of pH, *J. Phys.: Condens. Matter* 24 (12) (2012) 124101.

[30] D. Argyris, T. Ho, D.R. Cole, A. Striolo, Molecular dynamics studies of interfacial water at the alumina surface, *J. Phys. Chem. C* 115 (5) (2011) 2038–2046.

[31] D. Argyris, A. Phan, A. Striolo, P.D. Ashby, Hydration structure at the  $\alpha$ -Al<sub>2</sub>O<sub>3</sub> (0001) surface: Insights from experimental atomic force spectroscopic data and atomistic molecular dynamics simulations, *J. Phys. Chem. C* 117 (20) (2013) 10433–10444.

[32] M.J. DelloStritto, S.M. Piontek, M.L. Klein, E. Borguet, Effect of functional and electron correlation on the structure and spectroscopy of the Al<sub>2</sub>O<sub>3</sub>(0001)-H<sub>2</sub>O interface, *J. Phys. Chem. Lett.* 10 (9) (2019) 2031–2036.

[33] M. DelloStritto, S.M. Piontek, M.L. Klein, E. Borguet, Relating interfacial order to sum frequency generation with ab initio simulations of the aqueous Al<sub>2</sub>O<sub>3</sub>(0001) and (1120) interfaces, *J. Phys. Chem. C* 122 (37) (2018) 21284–21294.

[34] S.M. Piontek, M. DelloStritto, B. Mandal, T. Marshall, M.L. Klein, E. Borguet, Probing heterogeneous charge distributions at the  $\alpha$ -Al<sub>2</sub>O<sub>3</sub>(0001)/H<sub>2</sub>O interface, *J. Am. Chem. Soc.* 142 (28) (2020) 12096–12105.

[35] S. Pezzotti, A. Serva, F. Sebastiani, F.S. Brigiano, D.R. Galimberti, L. Potier, S. Alfaro, G. Schwaab, M. Havenith, M.-P. Gaigeot, Molecular fingerprints of hydrophobicity at aqueous interfaces from theory and vibrational spectroscopies, *J. Phys. Chem. Lett.* 12 (15) (2021) 3827–3836.

[36] C. Contescu, J. Jagiello, J.A. Schwarz, Heterogeneity of proton binding sites at the oxide/solution interface, *Langmuir* 9 (7) (1993) 1754–1765.

[37] T. Ye, D. Wynn, R. Dudek, E. Borguet, Photoreactivity of alkylsiloxane self-assembled monolayers on silicon oxide surfaces, *Langmuir* 17 (15) (2001) 4497–4500.

[38] G. Lamour, A. Eftekhari-Bafrooei, E. Borguet, S. Souès, A. Hamraoui, Neuronal adhesion and differentiation driven by nanoscale surface free-energy gradients, *Biomaterials* 31 (14) (2010) 3762–3771.

[39] G. Lamour, A. Hamraoui, A. Buvailo, Y. Xing, S. Keuleyan, V. Prakash, A. Eftekhari-Bafrooei, E. Borguet, Contact angle measurements using a simplified experimental setup, *J. Chem. Educ.* 87 (12) (2010) 1403–1407.

[40] H. Li, T. Yan, K.A. Fichthorn, S. Yu, Dynamic contact angles and mechanisms of motion of water droplets moving on nanopillared superhydrophobic surfaces: A molecular dynamics simulation study, *Langmuir* 34 (34) (2018) 9917–9926.

[41] D. Zhang, Y. Wang, Y. Gan, Characterization of critically cleaned sapphire single-crystal substrates by atomic force microscopy, xps and contact angle measurements, *Appl. Surf. Sci.* 274 (2013) 405–417.

[42] Z. Zhu, Z. Yu, F.F. Yun, D. Pan, Y. Tian, L. Jiang, X. Wang, Crystal face dependent intrinsic wettability of metal oxide surfaces, *National Science Review* 8 (1).

[43] J. Drelich, E. Chibowski, Superhydrophilic and superwetting surfaces: Definition and mechanisms of control, *Langmuir* 26 (24) (2010) 18621–18623.

[44] M.-P. Gaigeot, M. Sprik, M. Sulpizi, Oxide/water interfaces: How the surface chemistry modifies interfacial water properties, *J. Phys.: Condens. Matter* 24 (12) (2012) 124106.

[45] L. Lutterotti, P. Scardi, Simultaneous structure and size-strain refinement by the rietveld method, *J. Appl. Crystallogr.* 23 (4) (1990) 246–252.

[46] K.C. Hass, W.F. Schneider, A. Curioni, W. Andreoni, The chemistry of water on alumina surfaces: Reaction dynamics from first principles, *Science* 282 (5387) (1998) 265–268.

[47] K.C. Hass, W.F. Schneider, A. Curioni, W. Andreoni, First-principles molecular dynamics simulations of H<sub>2</sub>O on  $\alpha$ -Al<sub>2</sub>O<sub>3</sub> (0001), *J. Phys. Chem. B* 104 (23) (2000) 5527–5540.

[48] H.J.C. Berendsen, D. van der Spoel, R. van Drunen, Gromacs: A message-passing parallel molecular dynamics implementation, *Comput. Phys. Commun.* 91 (1–3) (1995) 43–56.

[49] E. Lindahl, B. Hess, D. van der Spoel, Gromacs 3.0: a package for molecular simulation and trajectory analysis, *J. Mol. Model.* 7 (8) (2001) 306–317.

[50] D. Van Der Spoel, E. Lindahl, B. Hess, G. Groenhof, A.E. Mark, H.J.C. Berendsen, Gromacs: Fast, flexible, and free, *J. Comput. Chem.* 26 (16) (2005) 1701–1718.

[51] B. Hess, C. Kutzner, D. van der Spoel, E. Lindahl, Gromacs 4: Algorithms for highly efficient, load-balanced, and scalable molecular simulation, *J. Chem. Theory Comput.* 4 (3) (2008) 435–447.

[52] S. Pronk, S. Päll, R. Schulz, P. Larsson, P. Bjelkmar, R. Apostolov, M.R. Shirts, J.C. Smith, P.M. Kasson, D. Van Der Spoel, Gromacs 4.5: a high-throughput and highly parallel open source molecular simulation toolkit, *Bioinformatics* 29 (7) (2013) 845–854.

[53] S. Päll, M.J. Abraham, C. Kutzner, B. Hess, E. Lindahl, Tackling exascale software challenges in molecular dynamics simulations with gromacs, in: S. Markidis, E. Laure (Eds.), *Solving Software Challenges for Exascale*, Springer International Publishing, Cham, 2015, pp. 3–27.

[54] M.J. Abraham, T. Murtola, R. Schulz, S. Päll, J.C. Smith, B. Hess, E. Lindahl, Gromacs: High performance molecular simulations through multi-level parallelism from laptops to supercomputers, *SoftwareX* 1 (2015) 19–25.

[55] S. Nosé, M.L. Klein, Constant pressure molecular dynamics for molecular systems, *Mol. Phys.* 50 (5) (1983) 1055–1076.

[56] M. Parrinello, A. Rahman, Polymorphic transitions in single crystals: A new molecular dynamics method, *J. Appl. Phys.* 52 (12) (1981) 7182–7190.

[57] S. Nosé, A molecular dynamics method for simulations in the canonical ensemble, *Mol. Phys.* 52 (2) (1984) 255–268.

[58] W.G. Hoover, Canonical dynamics: Equilibrium phase-space distributions, *Phys. Rev. A* 31 (3) (1985) 1695–1697.

[59] B. Hess, P-lincs: A parallel linear constraint solver for molecular simulation, *J. Chem. Theory Comput.* 4 (1) (2008) 116–122.

[60] U. Essmann, L. Perera, M.L. Berkowitz, T. Darden, H. Lee, L.G. Pedersen, A smooth particle mesh ewald method, *J. Chem. Phys.* 103 (19) (1995) 8577–8593.

[61] R.T. Cygan, J.-J. Liang, A.G. Kalinichev, Molecular models of hydroxide, oxyhydroxide, and clay phases and the development of a general force field, *J. Phys. Chem. B* 108 (4) (2004) 1255–1266.

[62] H.J.C. Berendsen, J.R. Grigera, T.P. Straatsma, The missing term in effective pair potentials, *J. Phys. Chem.* 91 (24) (1987) 6269–6271.

[63] G.R. Quezada, R.E. Rozas, P.G. Toledo, Molecular dynamics simulations of quartz (101)-water and corundum (001)-water interfaces: Effect of surface charge and ions on cation adsorption, water orientation, and surface charge reversal, *J. Phys. Chem. C* 121 (45) (2017) 25271–25282.

[64] G.M. Torrie, J.P. Valleau, Nonphysical sampling distributions in monte carlo free-energy estimation: Umbrella sampling, *J. Comput. Phys.* 23 (2) (1977) 187–199.

[65] G.A. Tribello, M. Bonomi, D. Branduardi, C. Camilloni, G. Bussi, Plumed 2: New feathers for an old bird, *Comput. Phys. Commun.* 185 (2) (2014) 604–613.

[66] Z. Tan, E. Gallicchio, M. Lapelosa, R.M. Levy, Theory of binless multi-state free energy estimation with applications to protein-ligand binding, *J. Chem. Phys.* 136 (14) (2012) 144102.

[67] A.J. Patel, P. Varily, D. Chandler, S. Garde, Quantifying density fluctuations in volumes of all shapes and sizes using indirect umbrella sampling, *J. Stat. Phys.* 145 (2) (2011) 265–275.

[68] A.J. Patel, P. Varily, D. Chandler, Fluctuations of water near extended hydrophobic and hydrophilic surfaces, *J. Phys. Chem. B* 114 (4) (2010) 1632–1637.

[69] E. Virga, E. Spruijt, W.M. de Vos, P.M. Biesheuvel, Wettability of amphoteric surfaces: The effect of ph and ionic strength on surface ionization and wetting, *Langmuir* 34 (50) (2018) 15174–15180.

[70] D. Yang, M. Krasowska, R. Sedev, J. Ralston, The unusual surface chemistry of  $\alpha$ -Al<sub>2</sub>O<sub>3</sub> (0001), *Phys. Chem. Chem. Phys.* 12 (2010) 13724–13729.

[71] E. Forrest, R. Schulze, C. Liu, D. Dombrowski, Influence of surface contamination on the wettability of heat transfer surfaces, *Int. J. Heat Mass Transf.* 91 (2015) 311–317.

[72] C.U. Gonzalez-Valle, B. Ramos-Alvarado, Molecular dynamics simulations of wettability, thermal transport, and interfacial liquid structuring at the nanoscale in polar solid-liquid interfaces, *ACS Appl. Nano Mater.* 4 (4) (2021) 3821–3832.

[73] J. Monroe, M. Barry, A. DeStefano, P. Aydogan Gokturk, S. Jiao, D. Robinson-Brown, T. Webber, E.J. Crumlin, S. Han, M.S. Shell, Water structure and properties at hydrophilic and hydrophobic surfaces, *J. Annu. Rev. Chem. Biomol. Eng.* 11 (1) (2020) 523–557.

[74] E. Xi, R.C. Remsing, A.J. Patel, Sparse sampling of water density fluctuations in interfacial environments, *J. Chem. Theory Comput.* 12 (2) (2016) 706–713.

[75] N.B. Rego, A.J. Patel, Understanding hydrophobic effects: Insights from water density fluctuations, *Annu. Rev. Condens. Matter Phys.* doi:10.1146/annurev-connatphys-040220-045516.

[76] A.J. Patel, P. Varily, S.N. Jamadagni, H. Acharya, S. Garde, D. Chandler, Extended surfaces modulate hydrophobic interactions of neighboring solutes, *Proc. Natl. Acad. Sci. USA* 108 (43) (2011) 17678–17683.

[77] R.C. Remsing, T.T. Duignan, M.D. Baer, G.K. Schenter, C.J. Mundy, J.D. Weeks, Water lone pair delocalization in classical and quantum descriptions of the hydration of model ions, *J. Phys. Chem. B* 122 (13) (2018) 3519–3527, <https://doi.org/10.1021/acs.jpcb.7b10722>.

[78] A. Lizar, D. Chandler, Hydrogen-bond kinetics in liquid water, *Nature* 379 (1996) 55.

[79] A. Chandra, Effects of ion atmosphere on hydrogen-bond dynamics in aqueous electrolyte solutions, *Phys. Rev. Lett.* 85 (4) (2000) 768–771.

[80] R. Kumar, J.R. Schmidt, J.L. Skinner, Hydrogen bonding definitions and dynamics in liquid water, *J. Chem. Phys.* 126 (20) (2007) 204107, <https://doi.org/10.1063/1.2742385>.

[81] M.K. Ridley, D. Tunega, Insights on the structural and dynamic properties of corundum-water interfaces from first-principle molecular dynamics, *J. Phys. Chem. C* 125 (1) (2020) 295–309.

[82] P. Huang, T.A. Pham, G. Galli, E. Schwegler, Alumina(0001)/water interface: Structural properties and infrared spectra from first-principles molecular dynamics simulations, *J. Phys. Chem. C* 118 (17) (2014) 8944–8951.

[83] D. Laage, G. Stirnemann, F. Sterpone, R. Rey, J.T. Hynes, Reorientation and allied dynamics in water and aqueous solutions, *Annu. Rev. Phys. Chem.* 62 (1) (2011) 395–416, <https://doi.org/10.1146/annurev.physchem.012809.103503>.

[84] G. Stirnemann, S.R.-V. Castrillón, J.T. Hynes, P.J. Rossky, P.G. Debenedetti, D. Laage, Non-monotonic dependence of water reorientation dynamics on surface hydrophilicity: competing effects of the hydration structure and hydrogen-bond strength, *Phys. Chem. Chem. Phys.* 13 (2011) 19911–19917.

[85] D. Laage, T. Elsaesser, J.T. Hynes, Water dynamics in the hydration shells of biomolecules, *Chem. Rev.* 117 (16) (2017) 10694–10725.

[86] F. Sterpone, G. Stirnemann, D. Laage, Magnitude and molecular origin of water slowdown next to a protein, *J. Am. Chem. Soc.* 134 (9) (2012) 4116–4119, <https://doi.org/10.1021/ja3007897>.

[87] D. Laage, J.T. Hynes, A molecular jump mechanism of water reorientation, *Science* 311 (5762) (2006) 832–835.

[88] N. Schwierz, D. Horinek, R.R. Netz, Anionic and cationic hofmeister effects on hydrophobic and hydrophilic surfaces, *Langmuir* 29 (8) (2013) 2602–2614.

[89] E. Xi, V. Venkateshwaran, L. Li, N. Rego, A.J. Patel, S. Garde, Hydrophobicity of proteins and nanostructured solutes is governed by topographical and chemical context, *Proc. Natl. Acad. Sci. USA* 114 (51) (2017) 13345–13350.

[90] A.S. Kelkar, B.C. Dallin, R.C. Van Lehn, Predicting hydrophobicity by learning spatiotemporal features of interfacial water structure: Combining molecular dynamics simulations with convolutional neural networks, *J. Phys. Chem. B* 124 (41) (2020) 9103–9114, <https://doi.org/10.1021/acs.jpcb.0c05977>.

[91] X. Liu, J. Cheng, M. Sprik, X. Lu, R. Wang, Understanding surface acidity of gibbsite with first principles molecular dynamics simulations, *Geochim. Cosmochim. Acta* 120 (2013) 487–495.

[92] T. Thi Bao Le, C. Divine-Ayela, A. Striolo, D.R. Cole, Effects of surface contamination on the interfacial properties of co2/water/calcite systems, *Phys. Chem. Chem. Phys.* 23 (34) (2021) 18885–18892. doi:10.1039/D1CP01106E.